Optimal Embedded Sensor Placement for Spatial Variability Assessment of Stationary Random Fields

Franck Schoefs, Emilio Bastidas-Arteaga, Trung-Viet Tran

Please cite this paper as:

Schoefs F, **Bastidas-Arteaga E**, Tran T-V. (2017). Optimal Embedded Sensor Placement for Spatial Variability Assessment of Stationary Random Fields. *Engineering Structures*
https://doi.org/10.1016/j.engstruct.2017.08.070

Optimal Embedded Sensor Placement for Spatial Variability Assessment of Stationary Random Fields

Franck Schoefs[1], Emilio Bastidas-Arteaga[1,†], Trung-Viet Tran[1]
Université Bretagne Loire, Université de Nantes, GeM, Institute for Research in Civil and Mechanical Engineering, CNRS UMR 6183, Nantes, France

ABSTRACT

Structural reliability assessment is largely influenced by the spatial variability of material properties or defaults; however, there are still various challenges for their characterization and modeling. Structural Health Monitoring (SHM) could provide useful information in space and time for spatial variability characterization of material properties and mechanical solicitations; nevertheless, this challenge is arduous because of the large number of potential sensor positions of local disruptions/failures. This paper proposes a methodology to optimize the spatial distribution of embedded sensors used for spatial variability assessment of stationary random fields. The optimization criterion relies on the width of the confidence interval of statistics for the characteristics to identify. For sake of simplicity, the paper illustrates the method for one-dimensional problems. The proposed method is applied firstly to a numerical example were several hypothetical structural configurations that could be found in practice are studied. It is finally applied to two case studies (a reinforced concrete beam and a steel wharf) where water content and loss of steel thickness are respectively measured. The results show that the stationary property is useful to deduce the minimum quantity of sensors and their position for a given quality requirement. They also allow us to propose a criterion for defining if regular or non-regular spacing of sensors along the inspection zone is more appropriate depending on the component length and autocorrelation structure of the random field.

Keywords: spatial variability; confidence interval; inspection optimization; stationary field; Karhunen-Loève expansion; sensor spacing; Structural Health Monitoring.

1. INTRODUCTION

Structural serviceability and safety are influenced by the different sources of uncertainty involved during their whole lifetime: material properties, loading, measures, model, deterioration, etc. A probabilistic structural analysis that includes the more influential uncertainties is therefore paramount to minimize both failure risks and design and maintenance costs. Nowadays, there are significant advances in probabilistic modeling at the scale of a single section of the structure. However, various works have demonstrated that the reliability assessment for a given component is largely influenced by the spatial variability of material properties or defaults [1–7]. Although the consideration of spatial variability is essential for proper reliability assessment, there are still various challenges for their characterization and modeling.

Non-Destructive Testing (NDT) and Structural Health Monitoring (SHM) could provide useful information in space and time for spatial variability characterization of material properties and mechanical solicitations. Several studies focused on the use of NDTs for spatial variability characterization at a given time. For example, Nguyen et al [8,9] combined several NDT techniques, kriging and variograms to assess the spatial variability of concrete at different scales (point, local and global). Gomez-Cardenas et al. [10] proposed a two-step approach to optimize the number and position of ultrasound measures required to localize critical zones. More recently, Schoefs et al. [11] proposed a methodology to find an optimal inspection configuration (number and localization of NDT measures) that

[†]corresponding author: tel: +33 2 51 12 55 24, email: emilio.bastidas@univ-nantes.fr, Address: 2 Rue de la houssinière BP 92208 44322 Nantes Cedex 3 France.

minimizes the error of identification of probability distributions for a given quantity of interest (resistance, porosity, water content, etc.) with spatial dependency. When an adaptive procedure can be selected on site for NDT, SHM requires a predefined design of embedded sensors positions. The main advantage of SHM relies on its capability to characterize the evolution in time of this spatial variability. Most part of research efforts in SHM have focused on the spatial localization of defects or damage of structural components [12–14]. However, spatial variability characterization of loading or material properties from SHM data is still a challenge because of the finite number of sensors and the large number of potential positions of local failures or disruptions. Numerical algorithms and specific multi-sensor systems should be developed towards this aim.

Within this framework, the main objective of this paper is to propose a methodology to optimize the spatial distribution of embedded sensors used for spatial variability assessment of stationary random fields. Stationary random fields have a stochastic structure and probabilistic properties that could be used to provide rational aid tools for optimizing the number and location of sensors. The paper shows that the stationary property of random fields is sufficient to achieve the optimal quantity of sensors and their position in view to provide a realistic characterization. The assessment of the shape of the Auto-Correlation Function (ACF) is paramount for spatial variability characterization. It is also essential to provide optimal measure positions for NDTs during inspection campaigns [11,15]. With respect to our previous work of focusing on NDTs [11], the main advantage of using embedded sensors for spatial variability characterization is that the stochastic properties are less sensitive to environmental conditions (sun, humidity, temperature, etc.) in depth leading to better assessment. Stochastic properties could also vary with time (e.g. for deterioration processes [16–18]); however, the evolution of spatial variability with time is beyond the scope of the present paper. In addition, since previous studies have shown that non-regular spacing of sensors is more efficient for identification purposes [19], non-regular sensor distributions will be considered in this study as a factor of optimization.

The paper starts in section 2 with a review of key concepts of spatial random field modeling with a focus on stationary random fields. Section 3 describes the proposed method for optimal sensors positioning in order to characterize the spatial correlation structure. This proposed strategy is illustrated with numerical examples (section 4) and real measurements on a reinforced concrete (RC) beam and a steel sheet-pile (section 5).

2. SPATIAL RANDOM FIELD MODELING

Random field theory provides a useful tool for spatial variability modeling. Among the different random field, a stationary stochastic process has been used in several applications [4–6,20–28] to represent spatial variability when the random field is considered homogeneous (symmetric field). These examples consider generally 1D stochastic processes. If 2D or 3D study cases are under consideration, the number of parameters to be identified increases (see section 2.3) but the methodology remains the same. This section summarizes the main assumptions and methods for stochastic modeling considered in this study. See [11] for more details.

2.1. Main assumptions for the stochastic modeling

In order to simplify the presentation of the proposed methodology, we consider the following main assumptions about the sensors and the random field modeling:

- The stochastic field is considered as: Gaussian, second order stationary, statistically homogeneous and its marginal distribution is known. This assumption implies that less information is required for its characterization.
- Each realization (single trajectory) represents the probabilistic information of all trajectories: mean, variance, spatial correlation. A single trajectory is then sufficient to describe the spatial variability, i.e. the stationary field is ergodic.
- A larger number of discrete sensors can be placed over the same component to characterize both randomness and spatial variability (e.g., from 20 to 60).
- Sensor measurements are considered as ‘perfect’ [15]. That means that (i) there is no bias and (ii) the error is insignificant or repetitive tests allow obtaining a good estimate of the real value and therefore to neglect the error. Nevertheless, if the error of the measure is well characterized, it could be also included in the analysis. This assumption helps to compute the inherent potential of the methodology and is consistent if the uncertainty on measurement is low. If it not the case, that will affects the estimation of the autocorrelation parameters and will lead to bad decisions with specific estimators. This aspect is beyond the scope of the paper.

2.2. Karhunen-Loève expansion

Given a probabilistic space (Ω, $\mathcal{F}$, P), a stochastic field or process with time or space is a collection of valued random variables indexed respectively by a set x "space" or t "time". Let us denote $Z(x,\theta)$ the one-dimensional stochastic field, where θ represents the randomness and x the spatial coordinate. $Z(x,\theta_i)$ is called the i^{th} sample function (or trajectory) of this field and corresponds to a given realization θ_i of the field for whatever location. $Z(x_1,\theta)$ is a random variable that is generated by θ at a given location $x = x_1$. Since we consider here only homogeneous random fields, the marginal distribution of $Z(x_1,\theta)$ does not depend on the location.

This paper uses a Karhunen-Loève expansion to model the stochastic field $Z(x,\theta)$ [29]. This expansion represents a random field as a combination of orthogonal functions on a bounded interval [$-a$, a]:

$$Z(x,\theta) = \mu_Z + \sigma_Z \sum_{i=1}^{n_{KL}} \xi_i(\theta) \sqrt{\lambda_i} f_i(x) \tag{1}$$

where μ_Z is the mean of the field Z, σ_Z is the standard deviation of the statistically homogeneous field Z, n_{KL} is number of terms in the expansion, ξ_i is a set of centered Gaussian random variables and λ_i and f_i are, respectively, the eigenvalues and eigenfunctions that depend on the type of ACF $\rho(\Delta x)$. It is possible to analytically determine the eigenvalues λ_i and eigenfunctions f_i for some correlation functions (see [11] or [30] for more details). For example, for an exponential ACF [31]:

$$\rho(\Delta x) = exp\left(\frac{-\Delta x}{b}\right), 0 < b \quad \text{and} \quad \Delta x = x_1 - x_2 \tag{2}$$

where b is an autocorrelation parameter and $\Delta x \in [-a, a]$. The spatial variability of various material properties or model parameters could be represented by an exponential autocorrelation. For instance, Jaksa et al. [26] used an exponential ACF to represent the spatial autocorrelation of the measurements from cone penetration tests measurements in Australia and other authors also recommend this model ([5,11]). Figure 1 illustrates how the exponential ACF provides a good fitting, according to Maximum Likelihood Estimate (see section 3.4), for representing the spatial variability of water content in a RC beam and corrosion in a steel sheet-pile. Generally speaking, the selection of the best ACF to represent the spatial variability depends on the intrinsic characteristics of the studied phenomenon. For simplicity, this study assumes that the random fields of the studied applications follow exponential ACFs. In case of homogeneous 2D or 3D random fields, equation (1) contains y and z coordinates with a unique value b to be identified. In case of non-homogeneous random fields, other parameters b_x, b_y, b_z in the 3D case will be estimated.

3. SENSOR PLACEMENT STRATEGY AND GOALS

3.1. Key ideas for sensor placement

The paper focuses on the assessment of the ACF of a stationary field. An optimal geo-positioning of sensors along a trajectory (sampling of the random field) (Figure 2-up) should provide an accurate assessment of the ACF parameters (i.e. b in eq. (2)) with a limited number of sensors. When looking for the usual shape of a correlation function (Figure 2-down) a regular spacing of sensors could not be optimal. If the distance between two sensors L_b is large the decay of autocorrelation for short distances cannot be assessed (e.g., 0m<distance<5m in Figure 2-down). On the contrary, if L_b is small, there is some information provided for many sensors that will not be useful for the assessment of b (e.g., distance>5m in Figure 2-down). Figure 2 shows that it is possible to install different number of sensors for high and low autocorrelation zones to obtain a good assessment of the autocorrelation parameter by reducing the total number of sensors N_s. The objective is to get a spacing of sensors providing a larger amount of data in the zone of high correlation. However, there is a limited feedback on the autocorrelation function (and consequently the value of b) for defining clearly the high autocorrelation zones. Section 4 presents a sensitivity study about the influence of the *a priori* knowledge of b. The following subsections describe the proposed procedure for determining the non-homogeneous spatial distribution of sensors.

3.2. Definition of the Spatial Correlation Threshold (SCT)

This paper considers a one-dimensional spatial field. The methodology could be applied on a set of trajectories representing: (i) a set of 1D components (beams), or (ii) a very long 1D-component

subdivided artificially or physically (expansion joint or construction joints) in a set of short components, or belonging to a wall structure (steel sheet pile or concrete wall).

In order to limit monitoring costs (number of sensors), we propose to monitor some zones of a trajectory with sensors separated by "*sufficiently short distance* L_b" allowing us to assess the shape of the ACF (eq. (2)) that is controlled by the parameter b. This "*sufficiently short distance*" can be seen as an Inspection Distance Threshold (IDT). Thus the non-regular distances of sensors spacing L_b^i should satisfy: $L_b^i \in]0, \text{IDT}[$ in the highly correlated zones.

The IDT is defined by assuming that, after a given distance, the events measured from an inspection can be assumed as weakly correlated. A Spatial Correlation Threshold (SCT) defines this weak correlation. For instance, Schoefs et al. [11] proposed a value SCT = 0.3 to get fairly correlated events and SCT = 0.5 to get high correlated events. For an exponential ACF, the SCT is linked with IDT by:

$$\text{IDT} = -b \cdot ln(\text{SCT}) \tag{3}$$

It was shown in [32] that a statistical error on the estimation of b can occur when limited measurements are available. Between the two values 0.4 and 0.5 and to increase the chance to get correlated values, this paper considers the value SCT = 0.4 to determine IDT. For example, for this value of SCT and b = 1.0 m, IDT = 0.92 m. The effect of this choice is discussed in [11].

3.3. Parameterization of the non-regular spacing

In view to reduce the set of potential solutions and simplify the design of the network of sensors, we propose a parameterization. It is based on a division of the trajectory (structural component) into n_p segments of same size L_m (see Figure 2) and then a subdivision of each segment into a decreasing N_c^i number of equidistant sensors, with distance L_b^i, following a series according to the octree approach. This approach has the advantage to get more information (more sensors) for small distances between points where the slope of the auto-correlation function must be fitted accurately. The number of sensors in the first segment is computed by:

$$N_c^1 = \text{Round}\left(\frac{N_s}{1 + \sum_{i=2}^{n_p} \frac{1}{2(i-1)}}\right) \tag{4}$$

The number of sensors for the segments $N_c^2, \ldots, N_c^{n_p-1}$ (i.e., N_c^i with $i \in [2;n_p–1]$) is estimated from:

$$N_c^i = \text{Round}\left(\frac{N_c^1}{2(i-1)}\right) \tag{5}$$

Since N_c^i should verify $N_s = \sum_{i=1}^{n_p} N_c^i$, the number of sensors for the last segment, $N_c^{n_p}$, is the remaining number of sensors:

$$N_c^{n_p} = N_s - \sum_{i=1}^{n_p-1} N_c^i \tag{6}$$

The only necessary inputs are the number of sensors N_s and the number of segments n_p. The distribution of sensors per segment is computed from equations (4) to (6). For instance, for 3 segments and 23 sensors, 13 sensors are placed in the first segment, 7 sensors in the second and 3 sensors in the last one. Figure 2 presents the distribution of sensors for this case.

Knowing the number of sensors in each segment, the distance between sensors in each segment is deduced as follows:

$$L_b^i = \begin{cases} \dfrac{L}{n_p(N_c^1 - 1)}, & \text{if } i = 1 \\ \dfrac{L}{n_p N_c^i}, & \text{otherwise} \end{cases} \tag{7}$$

To satisfy the condition of sufficient correlation between measurements (section 3.2), we should avoid a distance larger than IDT for the segments located in the high correlation zone (Figure 2). The length of this zone L_{hc} depends on the autocorrelation parameter b and could be estimated from eq. (2) by considering a low value of autocorrelation. For example, for b=1m $L_{hc} \approx –b$ ln(0.01) ≈ 4.6m. However, if

$L_b^i > IDT$ for the segments located in this high correlation zone, the total number of sensors, N_s, should be increased until ensuring this condition for a given number of segments.

This discretization technique fixes a deterministic shape of the sensor distribution with a given non-regular distribution of the lag. The objective now will be to optimize the number and position of sensors (number of segments) in view to reach a given quality on the estimation of the parameter of the ACF.

3.4. Parameter estimation, sensitivity analysis and optimization

Stationary stochastic fields are simulated by the Karhunen-Loève expansion (eq. (1)) assuming an exponential ACF (eq. (2)), whose parameter b has to be identified by knowing the two first statistic moments (μ_Z, σ_Z). Based on a continuous trajectory, for fixed values of N_s and n_p, we obtain a sample of discrete realizations from the sensor measurements $\hat{Z} = \{z_1, z_2, \dots, z_{N_s}\}$ corresponding to the sensors positions $X = \{x_1, x_2, \dots, x_{N_s}\}$ following the discretization procedure presented in section 3.3. Discrete values of the auto-correlation function are deduced from $\hat{Z}$ and given by [25]:

$$\rho_k = \frac{\sum_{i=1}^{N_s-k}(z_i - \mu_Z)(z_{i+k} - \mu_Z)}{\sum_{i=1}^{N_s}(z_i - \mu_Z)^2}, with\ 0 \le k \le N_s \tag{8}$$

We assess the value of b by using the Maximum Likelihood Estimate method (MLE), reported by Li [3]. The principle of the method is to find the best parameter (i.e. b in eq. (2)) for a given ACF candidate that gives the best fit to the experimental autocorrelation (eq. (10)) with respect to MLE estimate. This last one is better that the least square method that can lead to a biased estimation when data are lacking. The MLE for the estimation of b is computed by following the steps described by Kenshel [33] from:

$$L_h = \prod_{i=1}^{N_s}\left(\frac{1}{\sqrt{2\pi}} exp\left(\frac{-v_i^2}{2}\right)\right) = \left(\frac{1}{\sqrt{2\pi}}\right)^{N_s} exp\left(\frac{-\sum_{i=1}^{N_s} v_i^2}{2}\right) \tag{9}$$

where ν_i is the i^{th} component of the vector of independent standard values obtained from:

$$\boldsymbol{v} = \mathbf{C}^{-1}\left(\frac{\hat{Z} - \mu_{\hat{Z}}}{\sigma_{\hat{Z}}}\right) \tag{10}$$

where $\hat{Z}$ is the vector of realizations of the random variable Z from sensor measurements and $\mathbf{C}$ a lower triangular matrix such that $\mathbf{C}\mathbf{C}^{\mathrm{T}} = \boldsymbol{\rho}$ and $\boldsymbol{\rho}$ the auto-correlation matrix. Besides, maximize L_h is equivalent to minimize L_1:

$$L_1 = \sum_{i=1}^{N_s} v_i^2 \tag{11}$$

The estimated parameter of the auto-correlation function, $\hat{b}$, is then obtained by solving:

$$\hat{b} = \underset{b \in R^+}{\arg min} \sum_{i=1}^{N_s} v_i^2 \tag{12}$$

To account for the effect of random shape of trajectories, the analysis is carried out over a database containing 10,000 trajectories generated by Monte-Carlo simulations. This allows estimating 10,000 values $\hat{b}$ for each distribution of the sensor – i.e. one set of the couple (N_s, n_p). Note that in case of non homogeneous random fields, other parameters b_x, b_y, b_z in the 3D case, will be estimated from equation (12).

We select in this paper a confidence interval of the mean $\mu_{\hat{b}}$ expressed as a percentage Δ of the theoretical (true) value b^{th} to evaluate the quality of the SHM. From the 10,000 Monte-Carlo simulations we estimate the bounds of the confidence interval and the probability $P_{I,b}$ to get values inside the confidence interval, from the monitoring data. In a reliability study, $P_{I,b}$ will be discussed according to the requirements on the accuracy of the probability of failure assessment [23]. Thus we focus on the quality estimator:

$$P_{I,b} = P(\mu_{\hat{b}} \in [(1-\Delta)b^{th}, (1+\Delta)b^{th}]) \tag{13}$$

where $\mu_{\hat{b}}$ is the mean value of $\hat{b}$ computed from 10,000 Monte-Carlo simulations:

$$\mu_{\hat{b}} = \frac{1}{10{,}000} \sum_{k=1}^{10{,}000} \hat{b}_k \tag{14}$$

We define another estimate ε_b, the normalized quadratic error of the parameter $\hat{b}$:

$$\varepsilon_b = \left(\frac{\hat{b} - b^{th}}{b^{th}} \right)^2 \tag{15}$$

Note that $P_{I,b}$ is sensitive to N_s, n_p and the ratio IDT/L (Eqs. (6)-(10)). We analyze in the following this sensitivity by varying the number of sensors (N_s), the number of segments (n_p) and the ratio IDT/L. Finally, the optimal position and number n_p^{opt} of sensors is obtained by:

$$n_p^{opt} = \underset{n_p}{Arg\max} \{ P_{I,b}(N_s) \} \tag{16}$$

A numerical application will be presented in the next section to illustrate this sensitivity analysis.

4. APPLICATION TO A NUMERICAL STUDY CASE

4.1. Reference case: presentation, results and discussions

For illustrating the methodology and generalization purposes, it is considered in the following sections a set of 1D-components (beams) with a very large total length $L>>b$. The case of components with a limited size is discussed in section 4.2, excepting those where $L < L_b$ for which it is theoretically impossible to identify fully the stochastic field. The Gaussian stationary stochastic field is characterized by: the theoretical auto-correlation parameter b^{th}=1m, IDT=0.92m from eq. (3), μ_Z = 100 and σ_Z = 20. The objective is to optimize the position of sensors in view to reach a good assessment of the auto-correlation parameter b for an error $\Delta = 10\%$.

We first analyze the effect of the number of segments (n_p) on the quality of assessment defined according to (eq 16) for the reference case: large number of sensors N_s and large length L; namely N_s=200 and L=100m. We vary the number of segments from 1 (200 sensors equally separated by the distance L_b = IDT) to 20 (72, 36, 18, 12, 9, 7, 6, 5, 5, 4, 4, 3, 3, 3, 3, 2, 2, 2, 2, and 2). Figure 3a presents the evolution of the quality estimator ($P_{I,b}$) with n_p for 10,000 simulated trajectories. The regular spacing obtained for n_p=1 is shown to be not optimal whereas the optimum is found for n_p=2 with 133 sensors spaced 37.8 cm in the first segment of 50m and 67 sensors with spacing equal to 74.6cm in the second segment. Figure 3 presents other results to improve the understanding of the causes of this trend. Figure 3b plots the evolution with n_p of the two first statistics (mean and standard deviation) and the minimum and maximum values obtained for b from a sample of size 10,000. It is observed that the mean value decreases slightly with n_p and becomes stable with a significant bias in comparison to the reference theoretical value (1m). This means that identification algorithm underestimates the value of b. Thus, even if the standard deviation decreases with n_p, $P_{I,b}$ is not optimal for high values of n_p. Note that the maximum and minimum bounds are not symmetrical to the mean; Figure 4 illustrates the non-symmetrical distribution of b for a fixed sensor distribution. Figure 3c presents the potential relative error ε_b that can reach 4.8 (near 500%) for one realization upon 10,000. The results on Figure 3d show the mean and standard deviation of ε_b and confirm that the error on the mean governs the level of the quality estimator $P_{I,b}$ where the minimum value of the mean error is obtained for n_p=2. Figure 3d also indicates that there is a significant reduction of the standard deviation of the error from n_p=1 to 2.

We focus now on the effect of small perturbations around the value of b on the optimal solution. This is a key issue for studying the robustness of the solution obtained from an *a priori* value of b. This sensitivity analysis studies the effect of b on the error ε_b by assuming that b takes the following values around the reference one (i.e., b=1m): 0.8, 0.9, 1, 1.1, and 1.2 m (Figure 5). In the future, more and more data will be available to reduce the uncertainty on the value of b at the design stage as it is already the case for concrete strength for instance, depending on the material parameter of interest, the characteristics of the material, the exposure and on the building process; by focusing on concrete only, large ongoing experimental campaigns are carried out [34] and since only 4 years, more and more researchers are focusing on this challenging issue [5,10,11,23]. That is why we assume a uniform distribution for b with a coefficient of variation of 11%. Figure 5a plots the mean of the error ε_b for various values of n_p and b. It is found that the minimum error corresponds to n_p = 2 for all values of b. Figure 5b shows that the standard deviation of the error is sensitive to b for n_p = 2 and that leads to a given value for n_p > 5. Figure 5c presents the mean and standard deviation of the error for n_p = 2. It is noted that the error on the mean is almost constant with a minimum for b=1m but the error on the standard deviation increases with b. It is possible to conclude from this trend that under-estimating slightly the value of b reduces the error. This

study illustrate that the methodology is robust even if an error of the future value of b occurs at the design stage. The variability of correlation parameter on a given structure must be estimated by on-going works (see [34] for concrete in sea exposure for example).

4.2. Case of small structures: sensitivity of IDT/L

In the reference case, L and b were respectively of 100 m and 1 m and L>>b. This section analyzes the optimal position of sensors for smaller structures, for fixed b; therefore, we investigate the sensitivity of IDT/L on the quality estimators. For illustration purposes, we keep a large amount of sensors N_s (N_s=200 sensors). Figure 6a and Figure 6b present respectively the effects of six IDT/L ratios on the probability of interval $P_{I,b}$ and the mean of ε_b. It is shown that the probability of interval $P_{I,b}$ decreases when n_p increases and that for large values of IDT/L = 0.2 the probability reaches 0. This result means that the estimation of b is then not possible whatever n_p because for IDT/L = 0.2 the length of the structural component is too short to identify the spatial variability (see Figure 2). Figure 6b confirms this finding where mean of the error ε_b is larger than 40% for IDT/L =0.2. For different values of IDT/L, it is interesting to note that the non-regular spacing offers a benefit only when IDT/L remains below 0.03 and that n_p=2 is optimal in all these cases. As a conclusion, if the length of the monitored structure is small (L < 40 IDT) the identification error is large and the regular spacing with L_b = IDT should be recommended. On the contrary for $L \geq 40$ IDT, the non-regular spacing with the optimized number of segments n_p=2 reduces the identification errors.

4.3. Case of limited number of sensors

Previous sections considered a large amount of sensors (N_s = 200). However, in real cases, the number of sensors is limited for technical or economical reasons. We analyze now the effect of limited quantity of sensors by varying their number from 20 to 200. The corresponding results are plotted on Figure 7 and Figure 8, respectively for two cases IDT/L=0.01 (non-regular spacing for long components) and IDT/L=0.04 (regular spacing for short components). It is observed in Figure 7 that the probability of interval $P_{I,b}$ depends on both N_s and n_p. The interest of implementing a non-regular spacing is significant only if the number of sensors is large (N_s > 60) where the optimal number of segments is n_p=2. Moreover the gain in quality estimator from N_s =80 to 200 is not significant. For a smaller number of sensors (N_s < 60) one segment (n_p=1) maximizes $P_{I,b}$: the mean of ε_b is minimum and is stable on the range $1 \leq n_p \leq 5$ for N_s = 60 and $1 \leq n_p \leq 9$ for N_s = 40. On the overall it is noted that a good assessment could obtained for $2 \leq n_p \leq 6$. By deducing an envelope curve from Figure 7, it is possible to plot on Figure 9 an optimal zone of the couple (N_s, n_p) that could be used to determine the number of sensors to install.

Figure 8 gives the result for the second case IDT/L=0.04. The results confirm the findings of the previous section for short components where a regular spacing (L_b = IDT) should be recommended. Moreover, it is also shown that the gain in quality estimator is not significant for N_s varying from 50 to 200.

Figure 10 summarizes these results by plotting the optimum values of probability of interval $P_{I,b}$ and the mean ε_b with N_s for two ratios: IDT/L=0.01 (non-regular) with n_p=2 and IDT/L=0.04 (regular) with n_p=1. That illustrates more clearly the convergence of results with N_s and that the minimum recommended value could be N_s=60 sensors.

5. ILLUSTRATION FOR A REAL STUDY CASE

This section applies the proposed methodology and previous findings to two study cases for which real spatially distributed data are available:

- Inspection of the water content along a 16m length reinforced concrete beam placed on the site of IFSTTAR Laboratory, Nantes, France [11]. The measurements were carried out by using a capacitive NDT tool.
- Ultrasonic inspection of the corrosion depth on a corroded 10m length steel sheet-pile of gabion-type wharf in Boulogne, France.

Even if embedded sensors did not perform these measurements, these real data are very helpful to validate the proposed approach.

5.1. Data and modeling

Figure 11 presents the spatial measurements (trajectories) of the water content (RC beam) and corrosion depth (steel sheet-pile). Some values of the corrosion depth trajectory are lacking due mainly to error of

measurements and difficulties to measure at specific points during the inspection campaign. For these two trajectories, it is possible to compute the mean and standard deviation for each quantity of interest:

- μ_W = 6.3%, σ_W = 0.67% for the RC beam (computed from a sample of 80 measurements every 20 cm), and
- μ_{Cr} = 1.39 mm, σ_{Cr} = 0.64 mm for the steel sheet-pile (computed from a sample of 1,517 measurements spaced on average every 6.5 mm).

Figure 1 presents the computed autocorrelation values. We obtain a classical shape including negative values [25]. Applying the procedure described in section 3.4 it was found that the exponential correlation functions are appropriate to model the empirical values. The following parameters of the autocorrelation function (eq. 2) were estimated: b_W = 0.42m (RC beam) and b_{Cr} = 0.11m (steel sheet-pile). These results are assumed in the following results and discussions as the theoretical values.

Based on the fitted auto-correlation functions, the Inspection Distance Thresholds (IDT) are: IDT_W = 0.39m (RC beam) and IDT_{Cr} = 0.1m (steel sheet-pile). Taking into account the length of the structural components and the findings of section 4, it is possible to propose two types of sensors spacing:

- a regular spacing of measurements for the RC beam because the ratio IDT_W/L=0.39/16=0.025≥1/40; and
- a non-regular spacing for the steel sheet-pile because the ratio IDT_{Cr}/L = 0.1/12 < 1/40.

The following section compares real and numerical estimations to determine the appropriateness of the proposed sensor spacing in each case.

5.2. Comparison with real databases

This section estimates the errors on the identification of ε_b for both real data and simulations for the two study cases. Numerical simulations are based on: (i) the procedures described in section 2 to generate trajectories, and (ii) the values of mean, standard deviation and autocorrelation parameter identified in section 5.1. The main goal of this section is to validate the proposed numerical approach as well as to verify if the practical recommendations of the numerical findings of section 5.1 could be applied to real measures.

Figure 12a compares the evolution of the error of the assessment of b by considering various n_p for results obtained from simulations and those computed from real data measured on the RC beam. The numerical mean as well as the minimum and maximum values were computed from 10,000 simulations. The results show that the numerical and mean values are close and that ε_b is minimum for n_p = 1. This behavior confirms the recommendation based on the numerical findings for the case of L < 40IDT where the regular spacing is suggested in such a case. Figure 12b compares the evolution of the mean of ε_b with N_s for n_p=1 and n_p=2. It is observed that the mean of ε_b decreases when more information from additional sensors is considered. There is a convergence in the error that is faster when n_p=1; in such a case it is reached for N_s > 30 sensors. The results also show that a regular spacing with n_p=1 leads to lower error for both simulated and real data.

Figure 13 plots similar results to those presented in Figure 12 for the steel sheet-pile. Figure 13a confirms that the non-regular spacing is appropriated to reduce ε_b in this case where $L \geq$ 40IDT. Figure 13b shows the effect of the numbers of sensors N_s on the mean of ε_b. Results on Figure 13 indicate that the error is lower for n_p=2. They also show that there is a convergence trend for the mean of ε_b when the number of sensor increases; in this case it can be concluded that N_s=45 sensors are sufficient to satisfy the quality requirement.

6. CONCLUSIONS

SHM of new structures is increasing and offers an opportunity for using embedded sensors for uncertainty and spatial variability quantification. Information provided by SHM will be also very useful to plan destructive and NDT measurements for assessing supplementary data required for improving lifetime assessment and optimizing maintenance actions. This paper proposed an original method for defining a non-regular spacing of sensors devoted to the assessment of the autocorrelation function parameter of stationary fields. The method is based on the probabilistic identification of the autocorrelation function parameter and aims at reducing the error on its estimation. Numerical simulations of Gaussian stationary stochastic fields illustrate the potential of the method by providing a decision aid tool when a limited number of sensors is available. Based on these numerical results, it was found that the position of sensors is a key factor for estimating the autocorrelation function parameter. This methodology requires an a priori knowledge of the ACF which might be difficult to obtain before installing the sensors even if

several experimental studies focus on spatial variability characterization; therefore, a sensitivity study showed that the methodology was robust with a tolerance on the exact value.

The main results allow to propose a criterion for regular or non regular spacing of sensors along the inspection zone depending on the component length and autocorrelation structure of the random field: (i) regular spacing is recommended for the case $L < 40$IDT, and (ii) non-regular spacing is suggested for the case $L \geq 40$IDT. The paper shows also the important role of the position of sensors in the estimation of the autocorrelation function parameter. Even if only two segments are shown to be sufficient in the 1D case, it helps to decrease the number and therefore the cost of sensors and data treatment and this gain will increase in the 2D case.

7. AKNOWLEDGEMENTS

The authors would like to acknowledge the Pays de la Loire Region for supporting the projects ECND-PdL and SI3M as well as the European commission for funding the DuratiNet EC Interreg project (http://www.duratinet.org).

8. REFERENCES

[1] Stewart MG. Spatial variability of pitting corrosion and its influence on structural fragility and reliability of RC beams in flexure. Structural Safety 2004;26:453–70.

[2] Li J, Masia MJ, Stewart MG, Lawrence SJ. Spatial variability and stochastic strength prediction of unreinforced masonry walls in vertical bending. Engineering Structures 2014;59:787–97. doi:10.1016/j.engstruct.2013.11.031.

[3] Li Y. Effect of spatial variability on maintenance and repair decisions for concrete structures. Delft University, Delft, Netherlands, 2004.

[4] Srivastava A. Spatial Variability Modelling of Geotechnical Parameters and Stability of Highly Weathered Rock Slope. Indian Geotechnical Journal 2012;42:179–85.

[5] O'Connor A, Kenshel O. Experimental Evaluation of the Scale of Fluctuation for Spatial Variability Modeling of Chloride-Induced Reinforced Concrete Corrosion. Journal Of Bridge Engineering 2013;18:3–14.

[6] Griffiths DV, Fenton GA. Influence of soil strength spatial variability on the stability of an undrained clay slope by finite elements. Slope Stability 2000 ASCE 2000:184–93.

[7] Pasqualini O, Schoefs F, Chevreuil M, Cazuguel M. Measurements and statistical analysis of fillet weld geometrical parameters for probabilistic modelling of the fatigue capacity. Marine Structures 2013;34:226–48. doi:10.1016/j.marstruc.2013.10.002.

[8] Nguyen NT, Sbartaï Z-M, Lataste J-F, Breysse D, Bos F. Assessing the spatial variability of concrete structures using NDT techniques – Laboratory tests and case study. Construction and Building Materials 2013;49:240–50. doi:10.1016/j.conbuildmat.2013.08.011.

[9] Nguyen NT, Sbartaï ZM, Lataste J-F, Breysse D, Bos F. Non-destructive evaluation of the spatial variability of reinforced concrete structures. Mechanics & Industry 2014;16:103. doi:10.1051/meca/2014064.

[10] Gomez-Cardenas C, Sbartaï ZM, Balayssac JP, Garnier V, Breysse D. New optimization algorithm for optimal spatial sampling during non-destructive testing of concrete structures. Engineering Structures 2015;88:92–9. doi:10.1016/j.engstruct.2015.01.014.

[11] Schoefs F, Bastidas-Arteaga E, Tran TV, Villain G, Derobert X. Characterization of random fields from NDT measurements: A two stages procedure. Engineering Structures 2016;111:312–22. doi:10.1016/j.engstruct.2015.11.041.

[12] Hu W-H, Thöns S, Rohrmann RG, Said S, Rücker W. Vibration-based structural health monitoring of a wind turbine system. Part I: Resonance phenomenon. Engineering Structures 2015;89:260–72. doi:10.1016/j.engstruct.2014.12.034.

[13] Ye XW, Ni YQ, Wong KY, Ko JM. Statistical analysis of stress spectra for fatigue life assessment of steel bridges with structural health monitoring data. Engineering Structures 2012;45:166–76. doi:10.1016/j.engstruct.2012.06.016.

[14] Kulprapha N, Warnitchai P. Structural health monitoring of continuous prestressed concrete bridges using ambient thermal responses. Engineering Structures 2012;40:20–38. doi:10.1016/j.engstruct.2012.02.001.

[15] Schoefs F, Clement A, Nouy A. Assessment of spatially dependent ROC curves for inspection of random fields of defects. Structural Safety 2009;31:409–19.

[16] Sheils E, O'Connor A, Schoefs F, Breysse D. Investigation of the effect of the quality of inspection techniques on the optimal inspection interval for structures. Structure and Infrastructure Engineering 2012;8:557–68. doi:10.1080/15732479.2010.505377.

[17] Bastidas-Arteaga E, Schoefs F. Stochastic improvement of inspection and maintenance of corroding reinforced concrete structures placed in unsaturated environments. Engineering Structures 2012;41:50–62. doi:10.1016/j.engstruct.2012.03.011.

[18] Bastidas-Arteaga E, Schoefs F. Sustainable maintenance and repair of RC coastal structures. Proceedings of the Institution of Civil Engineers - Maritime Engineering 2015;168:162–73. doi:10.1680/jmaen.14.00018.

[19] Schöberl M, Keinert J, Ziegler M, Seiler J, Niehaus M, Schuller G, et al. Evaluation of a high dynamic range video camera with non-regular sensor. IS&T/SPIE Electronic Imaging, 2013, p. 86600M--86600M.

[20] Bazant Z, Xi Y. Statistical Size Effect in Quasi-brittle Structures: II. Nonlocal Theory. ASCE J of Engrg Mech 1991;117:2623–40.

[21] Bazant Z, Novák D. Probabilistic Nonlocal Theory for Quasibrittle Fracture Initiation and Size Effect. I: Theory. Journal of Engineering Mechanics 2000;126:166–74.

[22] Bazant Z, Novák D. Probabilistic Nonlocal Theory for Quasibrittle Fracture Initiation and Size Effect. II: Application. Journal of Engineering Mechanics 2000;126:175–85.

[23] Stewart MG. Spatial Variability of Damage and Expected Maintenance Costs for Deteriorating RC Structures. Structure and Infrastructure Engineering 2006;2:79–96.

[24] Nobahar A. Effects of soil spatial variability on soil-structure interaction. PhD Thesis, Memorial University, St. John's, NL., 2003.

[25] Chenari RJ, Dodaran RO. New method for estimation of the scale of fluctuation of geotechnical properties in natural deposits. Computational Methods in Civil Engineering 2010;1:55–66.

[26] Jaksa MB. Experimental evaluation of the scale of fluctuation of a stiff clay. In: Melchers RE, Stewart MG, editors. Proc. 8th Int. Conf. on the Application of Statistics and Probability, Sydney: Balkema; 1999, p. 415–22.

[27] Pasqualini O, Schoefs F, Chevreuil M, Cazuguel M. Statistical analysis of welded joints geometry for stochastic modeling and reliability analysis. In: ASRANeT, editor. 6th Conference on Network for Integrating Structural Analysis, Risk and Reliability (ASRANet), London (UK): 2012.

[28] Ray A. Stochastic Measure of Fatigue Crack Damage for Health Monitoring of Ductile Alloy Structures. Structural Health Monitoring 2004;3:245–63. doi:10.1177/1475921704045626.

[29] Li C-C, Der Kiureghian A. Optimal Discretization of Random Fields. Journal of Engineering Mechanics 1993;119:1136–54. doi:10.1061/(ASCE)0733-9399(1993)119:6(1136).

[30] Ghanem RG, Spanos PD. Stochastic Finite Elements: A Spectral Approach. New York, USA: Springer; 1991.

[31] Vanmarcke E. Random fields: analysis and synthesis. Mass, London: MIT Press, Cambridge; 1983.

[32] Ravahatra NR, Duprat F, Schoefs F, de Larrard T, Bastidas-Arteaga E, Rakotovao Ravahatra N, et al. Assessing the capability of analytical carbonation models to propagate uncertainties and spatial variability of reinforced concrete structures. Frontiers in Built Environment 2017;3:1. doi:10.3389/FBUIL.2017.00001.

[33] Kenshel O. Influence of spatial variability on whole life management of reinforced concrete bridges. University of Dublin, Trinity College, Dublin, Ireland, 2009.

[34] Boureau L, Bouteiller V, Schoefs F, Gaillet L, Thauvin B, Schneider J, et al. On-site corrosion monitoring – reliability. International RILEM Conference on Materials, Systems and Structures in Civil Engineering - Conference segment on Electrochemistry in Civil Engineering, DTU, Lyngby, Denmark: 2016.

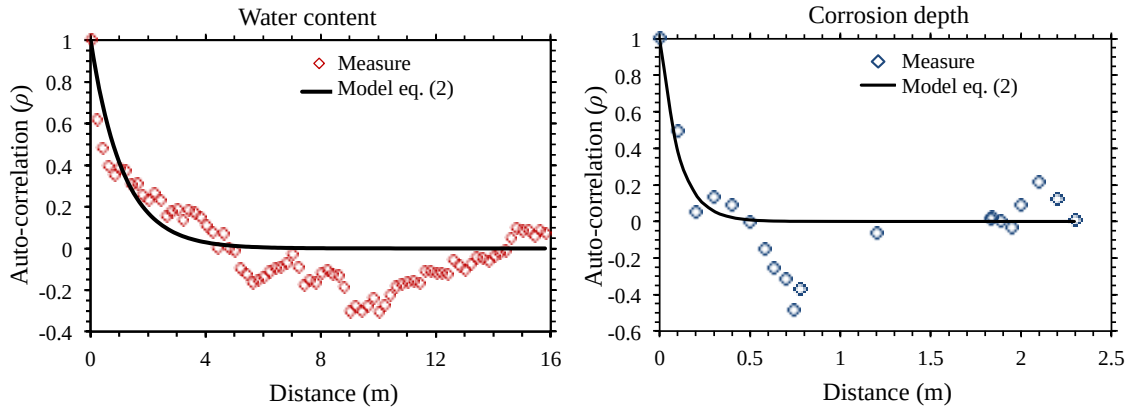

Figure 1. Auto-correlation data and fitted ACFs for water content in a RC beam (IFSTTAR, Nantes, France) and corrosion in a steel sheet-pile (Boulogne, France).

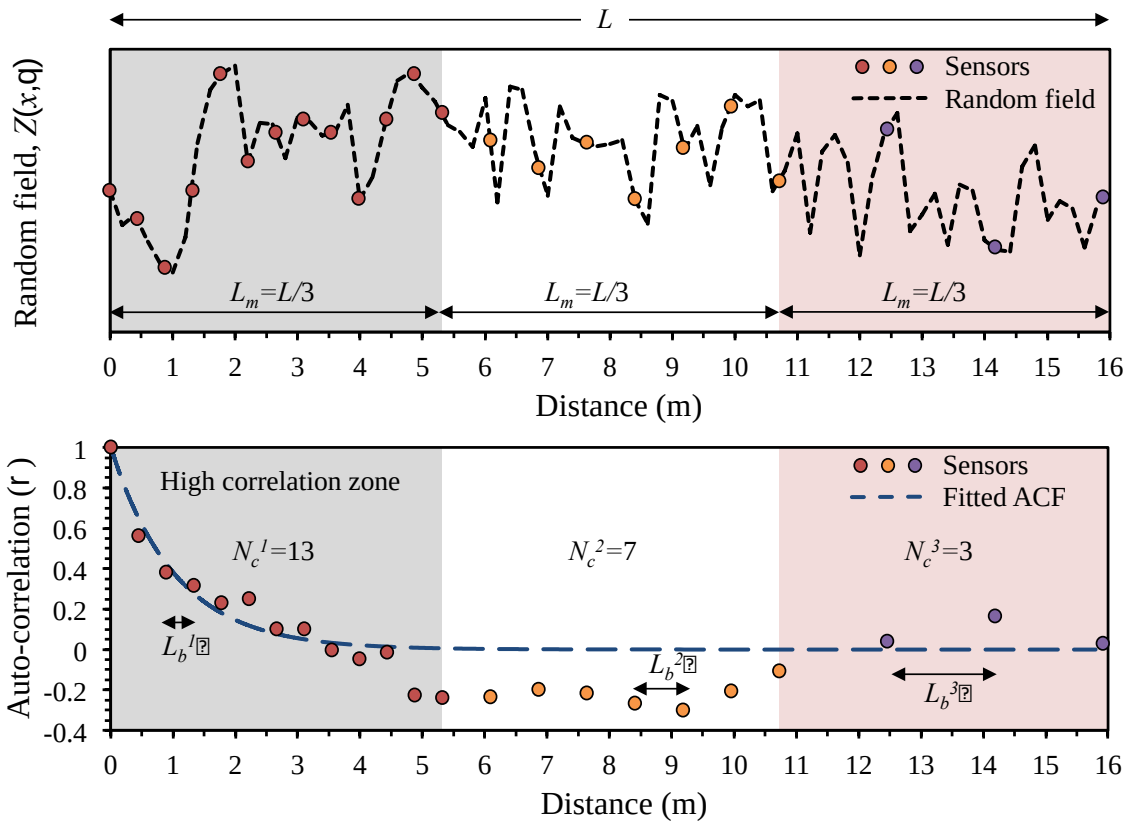

Figure 2. Representation of high correlation zones and non-regularly spacing sensors (N_s=23 sensors and n_p=3 segments) along a trajectory of the random field $Z(x, \theta)$ and estimated autocorrelation.

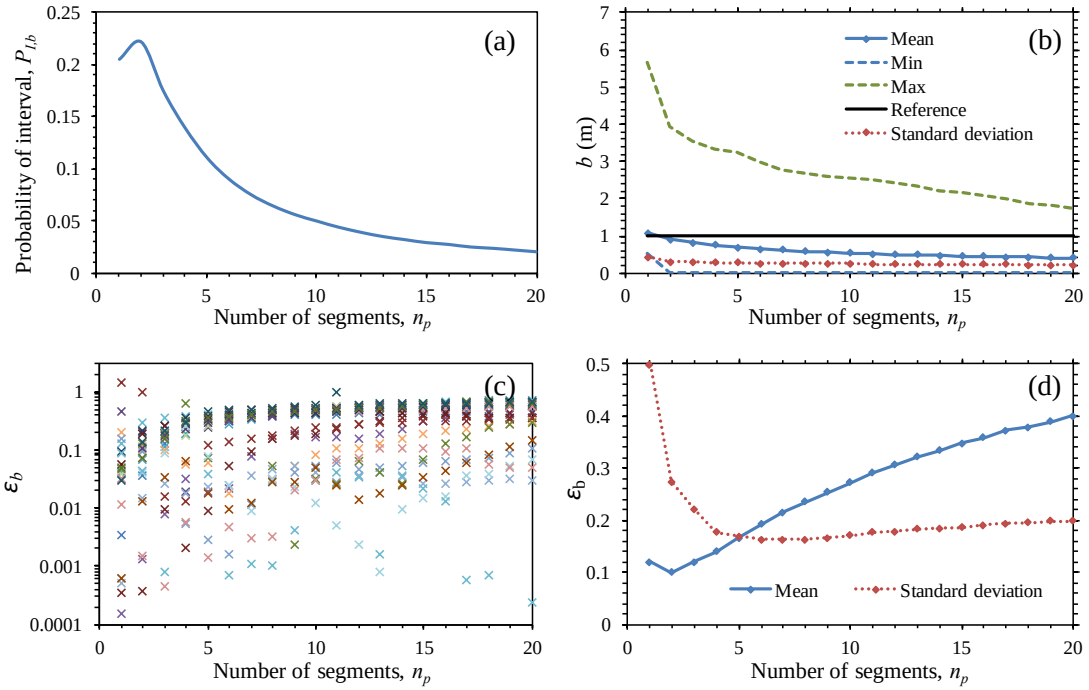

Figure 3. Effect of number of segments n_p on: (a) the probability of interval $P_{I,b}$, (b) the estimated values of the auto-correlation parameter b (c) the distribution of ε_b, and (d) the mean and standard deviation of ε_b (N_s=200, L=100m and Δ=10%).

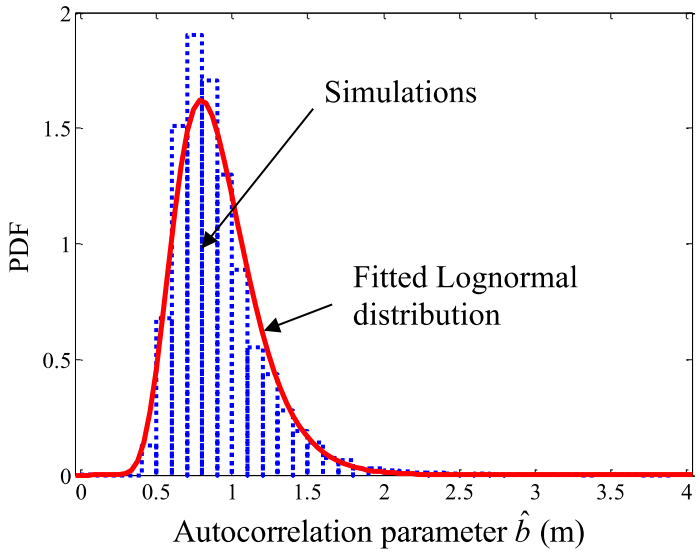

Figure 4. Distribution of estimated auto-correlation parameter $\hat{b}$ for N_s=200 and n_p=2.

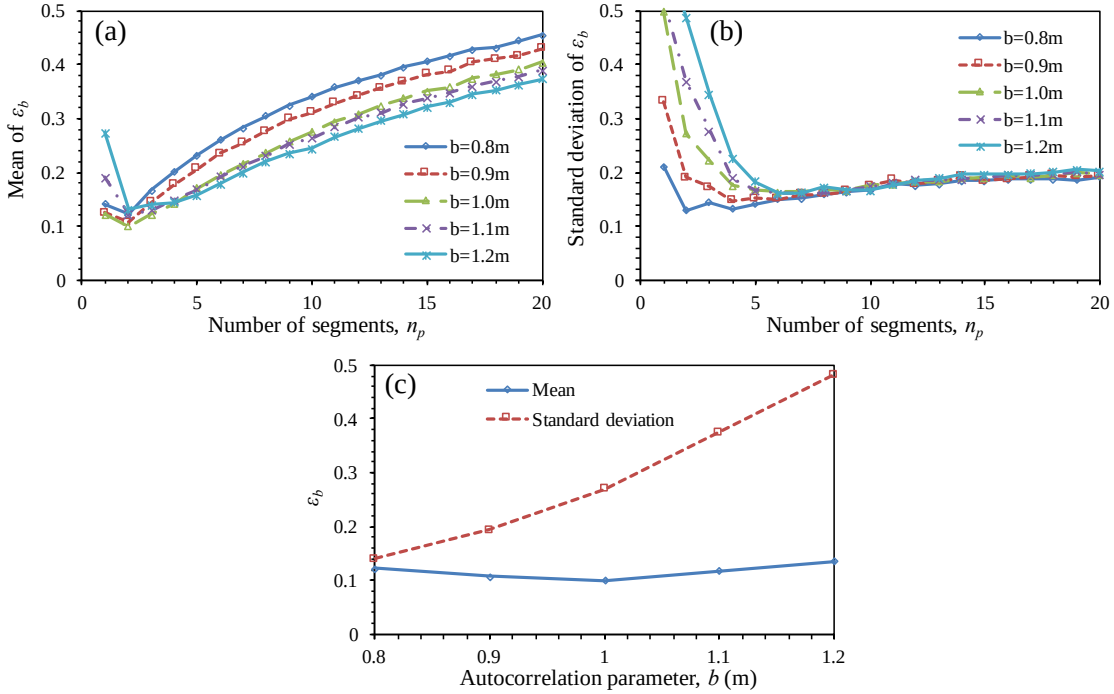

Figure 5. Sensitivity of ε_b for: (a) the mean of ε_b, (b) the standard deviation of ε_b, and (c) the mean and standard deviation of ε_b for n_p=2 (N_s=200, L=100m).

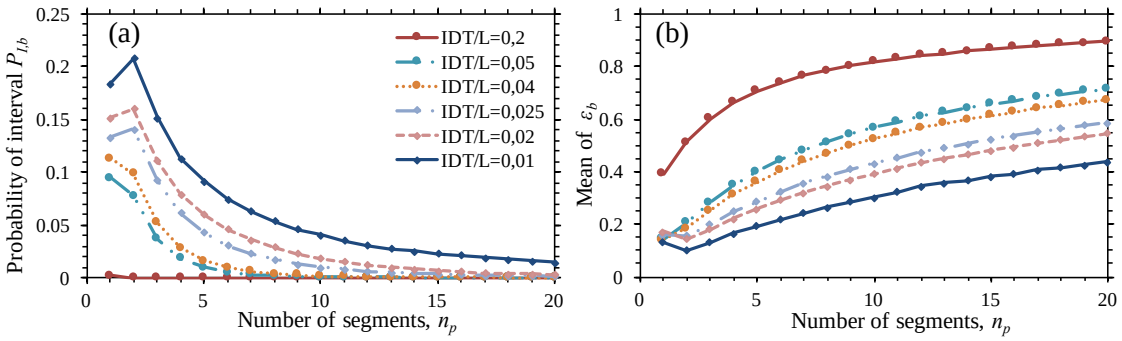

Figure 6. Effect of ratio IDT/L on (a) the probability of interval $P_{I,b}$, and (b) the mean of ε_b as a function of the number of segments n_p (N_s=200 and Δ=10%).

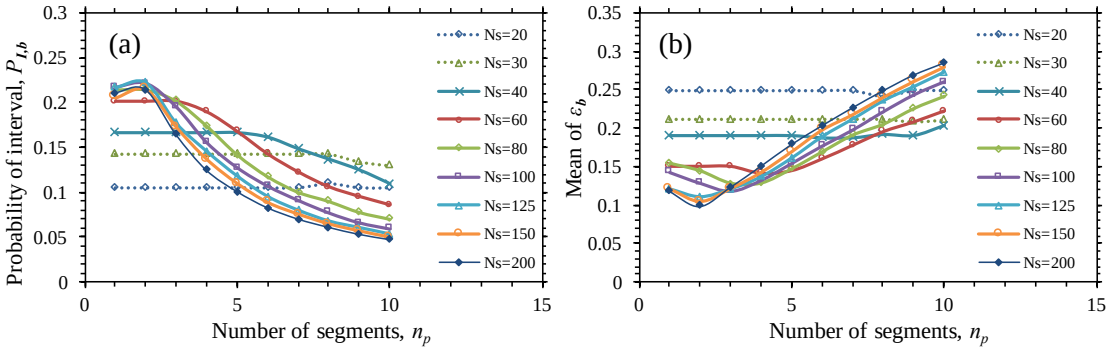

Figure 7. Effect of N_s on (a) the probability of interval $P_{I,b}$, and (b) the mean of ε_b, for various N_s (IDT/L=0.01 and Δ=10%).

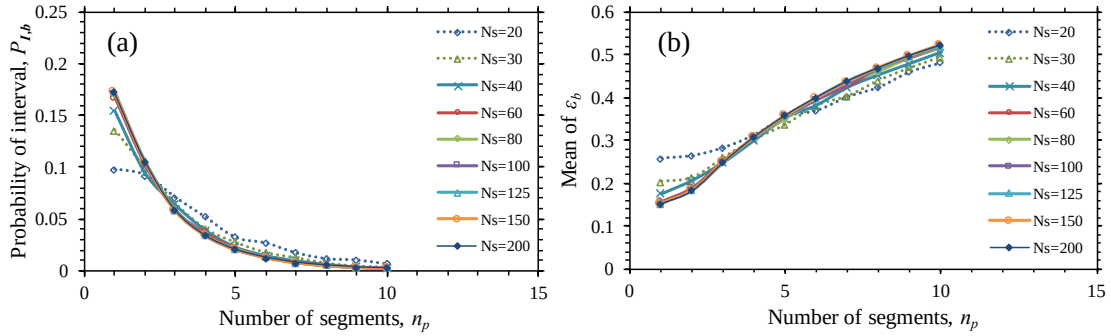

Figure 8. Effect of N_s on (a) the probability of interval $P_{I,b}$, and (b) the mean of ε_b, for various N_s (IDT/L=0.04 and Δ=10%).

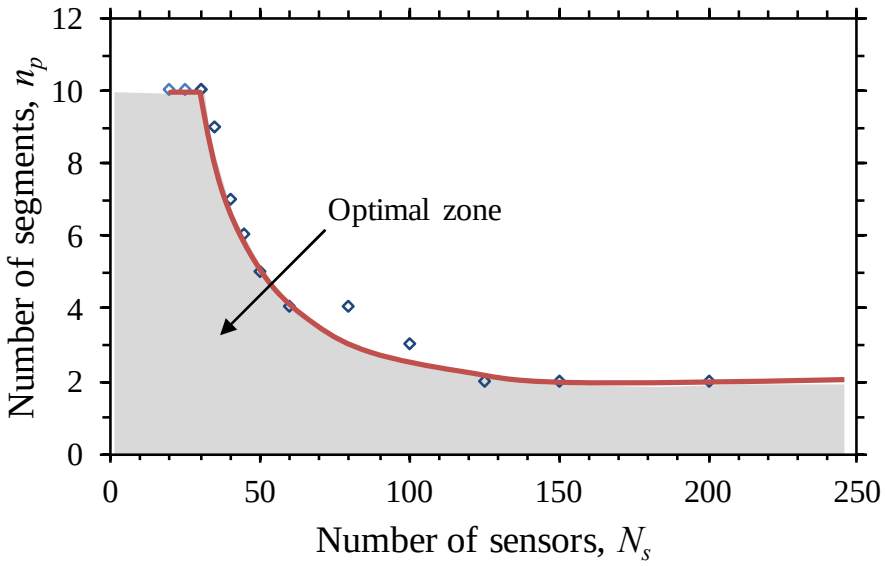

Figure 9. Definition of optimal zone for determining the number of sensors as a function of the number of segments (IDT/L=0.01 and Δ=10%).

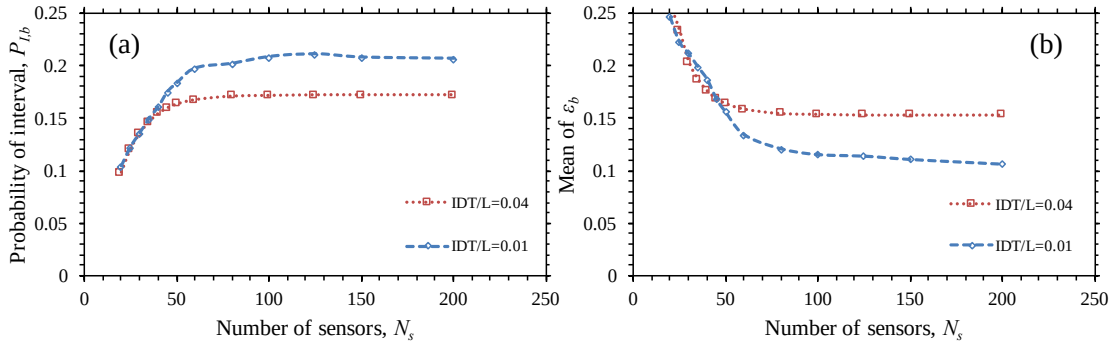

Figure 10. Effect of N_s on (a) the probability of interval $P_{I,b}$, and (b) the mean of ε_b, for Δ=10% and n_p optimized.

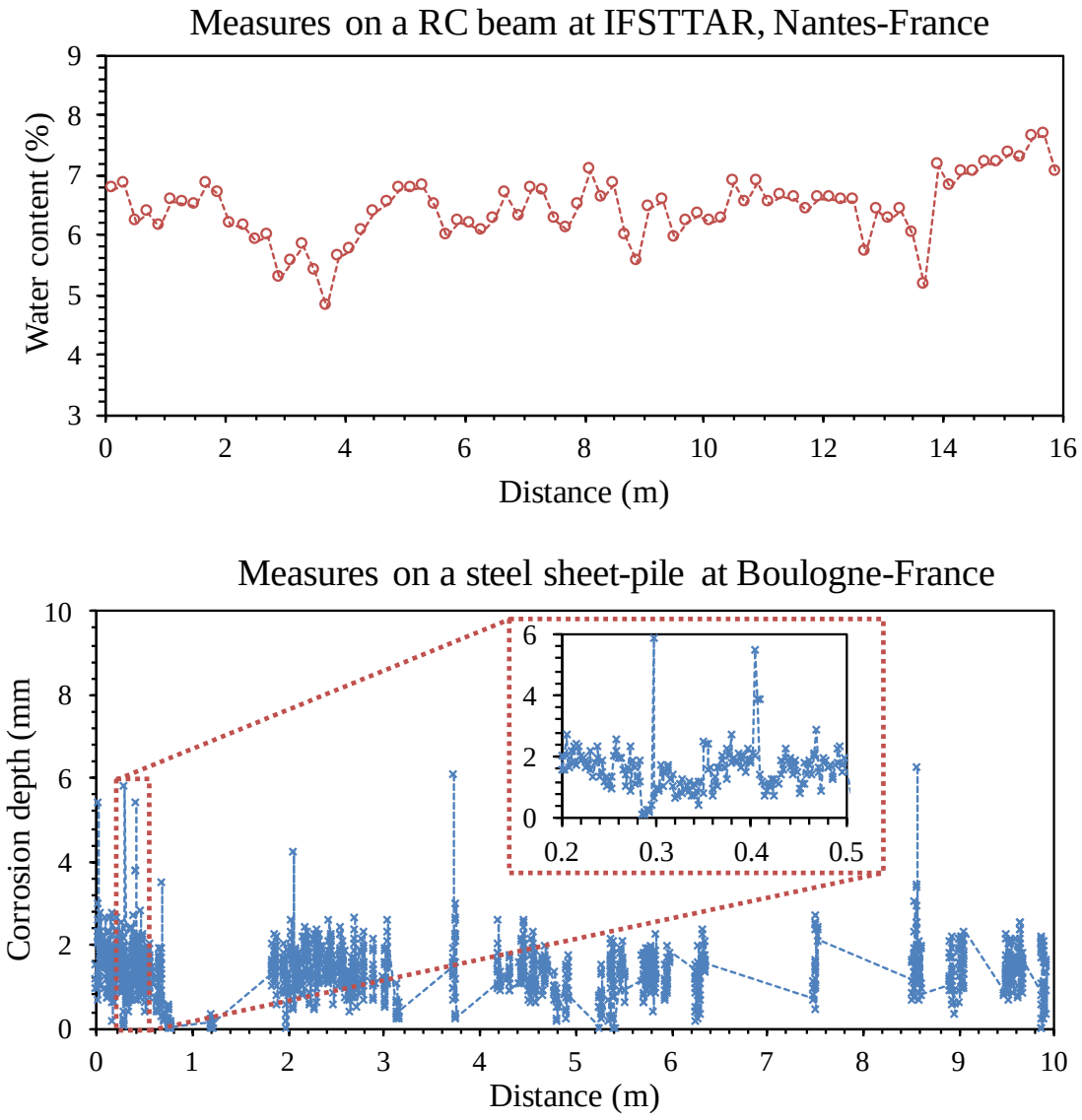

Figure 11. Experimental trajectories of water content (up) and corrosion (down).

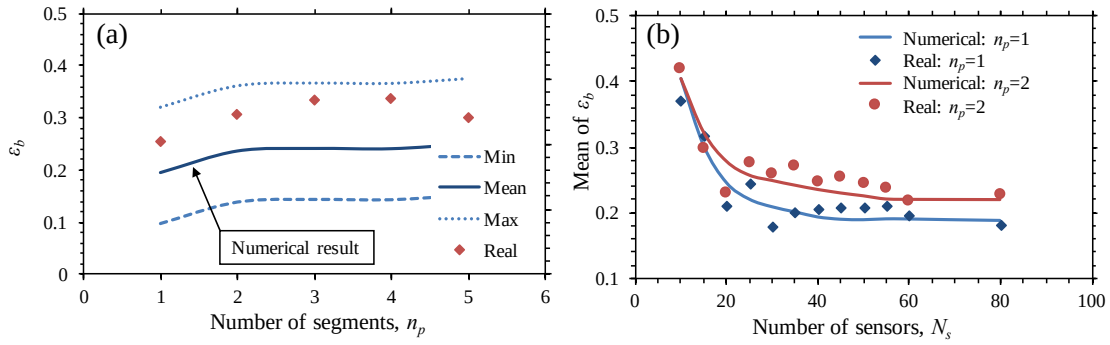

Figure 12. Comparison between simulated results and real inspection values in the case of water content (RC beam, L =16 m, IDT=0.4m): (a) effect of n_p on ε_b, for N_s=40 sensors (b) effect of N_s on the mean of ε_b.

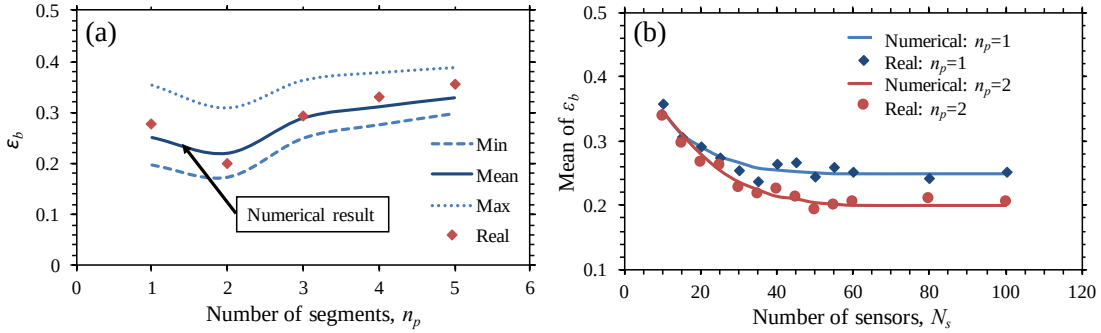

Figure 13. Comparison between simulated results and real inspection values in the case of corrosion depth (steel sheet-pile, L =12 m, IDT=0.1m): (a) effect of n_p on ε_b, for N_s=40 sensors (b) effect of N_s on the mean of ε_b.